



Common Mechanical Properties of Diffusion Bonded Joints and Their Corresponding Microstructure Features

Jiangtao Xiong, Yu Peng, Muhammad Samiuddin, Lin Yuan, and Jinglong Li

(Submitted August 29, 2019; in revised form February 27, 2020; published online May 4, 2020)

The mechanical properties of diffusion bonded joints embodied from 29 different kinds of alloys obtained from experiments (37 specimens) or literature (194 specimens) were analyzed and compared with their corresponding base alloys. The results indicated that toughness was most sensitive to the bonding quality as only 7.8% of the joints had a relative (ratio between the joint value and base alloy value) impact toughness of higher than 0.9, where the percentage of joints with a relative elongation (area reduction) and a tensile strength of higher than 0.9 was approximately only 21.9% and 48.4%, respectively. The fatigue and high-temperature mechanical properties of joints were significantly lower than those of the base alloys. Microstructure analysis revealed that this characteristic of “high strength–low toughness” resulted from defects of the joint, which included not only the widely accepted interfacial void defects but also the defects of the bond line and the crystallographic mismatch. Among these defects, the bond line primarily dispersed the plasticity and toughness of the joint. If the bond line was removed by post-bonding heat treatments or by insertion of an interlayer, the joint mechanical properties, particularly toughness, could potentially reach the value shown by the base alloy that had undergone the same heating process.

Keywords bond line, crystallographic mismatch, diffusion bonding, interfacial microvoids, mechanical properties

1. Introduction

Diffusion bonding is a precision solid welding method, which is employed in the high-tech manufacturing industry to fabricate complex and key structures, such as the hollow engine blades for aerospace applications (Ref 1,2), as well as the first wall and cooling plates for nuclear power generation (Ref 3,4). In 1964, Aerojet developed the platelet technology based on diffusion bonding to fabricate monolithic structures containing complex flow passages (Ref 5). This technology is used in solid additive manufacturing, i.e., laminated object manufacturing via diffusion bonding (LOM-DB), which consists of two steps: Firstly, metal sheets are chemically etched to form layered structures with completely and/or partially etched patterns, and these layered structures are then precisely stacked in a predetermined sequence and diffusion bonded together. LOM-DB was initially used in aerospace applications to produce structures comprising various features such as intricate inner manifolds, cooling passages, filters, precise metering orifices, and injector elements. (Ref 6-8). The development of computer-aided design/manufacturing has undoubtedly reduced the

overall cost of LOM-DB. Thus, this technology has been extensively adopted by many manufacturing companies (Ref 5,9-12), since it is an exceptional method for fabricating structures with inner passages. LOM-DB significantly promoted the application of diffusion bonding to precisely form more complex structures that were used in extreme environments, which included the sodium/CO₂ intermediate heat exchanger that was used for next-generation nuclear plants (Ref 9) and the high-temperature and pressure microchannel heat exchanger used for supercritical CO₂ Brayton cycles (Ref 9,11) or gas turbines (Ref 12). It is essential to completely understand the common mechanical properties of diffusion bonded joints and their corresponding microstructure features, which is not only the basis for evaluating the reliability of diffusion bonded structures, but also an important step for further broadening the applications of diffusion bonding, especially for LOM-DB. In other words, the mechanical properties of diffusion bonded joints depend upon their microstructural characteristics. In general, three types of microstructural features are observed in the interfacial area of diffusion bonded joints, which include interfacial microvoids, bond line, and crystallographic mismatch. If microvoids are present in the interface, the strength, elongation, and impact toughness of joints cannot be comparable to the base metal (Ref 13,14). Moreover, the precipitated phases such as oxides and carbides, along the joint, affect the mechanical properties of joints, especially the toughness; these phases were altered with bonding parameters (Ref 10,15-17). As for the crystallographic mismatch, it reduced the joint plasticity, high-temperature endurance performance (Ref 18), and fatigue performance (Ref 19).

In this study, the statistical method for the analysis of the mechanical properties of joints is represented in “[Method of Joint Property Evaluation](#)” section; further, the common features of these mechanical properties are analyzed in “[Common Features of the Joint Mechanical Properties](#)” section, and their corresponding microstructural features are

Jiangtao Xiong, Yu Peng, and Jinglong Li, State Key Laboratory of Solidification Processing, Northwestern Polytechnical University, Xi'an 710072, People's Republic of China; and Shaanxi Key Laboratory of Friction Welding Technologies, Northwestern Polytechnical University, Xi'an 710072, People's Republic of China; and **Muhammad Samiuddin and Lin Yuan**, Shaanxi Key Laboratory of Friction Welding Technologies, Northwestern Polytechnical University, Xi'an 710072, People's Republic of China. Contact e-mail: xiongjiangtao@nwpu.edu.cn.

discussed in “[Microstructure Features of Diffusion Bonded Joints](#)” section. Moreover, the improvement in these mechanical properties has been addressed in “[Improvement of the Joint Mechanical Properties](#)” section, and finally, the conclusion is provided in “[Conclusions](#)” section.

2. Method of Joint Property Evaluation

The sample space consists of 231 diffusion bonded joints (37 joints formed by our experiments and 194 joints collected from literature) produced by 29 different kinds of alloys (9 main categories), as shown in Table 1. But each of the joints is formed by the same alloy. Heterogeneous joints are not included in this study.

The mechanical property analysis mainly focused on tensile strength, elongation (or area reduction), and impact toughness at room temperature. The data associated with fatigue and high-temperature properties, although limited, were also analyzed. In order to extract the common features of diffusion bonded joints, the properties of each joint were represented by a relative property that is the ratio between the property of joint and that of the received base alloy. Table 1 lists the types and mechanical properties of the base alloy.

Using 231 samples, 37 joints were formed by our diffusion bonding experiments, which included 316L stainless steel (SN: 91-101), S136 mold steel (SN: 166-178), and TC4 titanium alloy (SN: 104-116). All of the diffusion bonding specimens were 35 mm in height and 45 mm in diameter. Acid pickling of the surfaces was done followed by ultrasonic cleaning in acid. The diffusion bonding processes were then performed in a vacuum furnace having vacuum $\leq 5 \times 10^{-3}$ Pa. The microstructure of the joints was observed by a scanning electron microscope (SEM, FEI Nova) equipped with an

electron backscatter diffraction (EBSD) system. Meanwhile, the bonded ratio was measured by the software Image-Pro Plus 6.0 according to the SEM images of joints. Equation (1) shows how to calculate the bonded ratio.

$$\eta = \left(\sum_{i=1}^n L_i/L \right) \times 100\% = \left(1 - \sum_{j=1}^m L_{\text{void}j}/L \right) \times 100\% \quad (\text{Eq 1})$$

The tensile specimens were machined according to the national standards of China GB/T 228.1-2010, and three tensile samples were measured for each bonding condition. Figure 1 shows the sampling locations and geometries of samples. The tensile test was performed using Instron 3382 with an initial strain rate of 1 mm min^{-1} .

3. Common Features of the Joint Mechanical Properties

Figure 2 shows the relative mechanical properties of 231 joints, which illustrates the distribution of normalized properties, i.e., relative tensile or shear strength (RTS or RSS), relative elongation (RE), relative area reduction (RAR), and relative impact energy (RIE). It indicates that strengths of diffusion bonded joints are generally satisfactory. Most of the strengths, i.e., RTS (or RSS), have values higher than 60%, the majority of which are around 100%, especially for reduced activation F/M steel and titanium alloy. But the RTS (or RSS) of intermetallic compound, Al, or Mg alloys barely reaches 100%. The plasticity, i.e., RE or RAR, is more dispersed than RTS (or RSS) that can be found not only at 100% but also at 0%. The RE or RAR values of ODS steel, intermetallic

Table 1 The types and mechanical properties of base alloy

Main category	Type, Specimen number (SN) and mechanical properties
Superalloy	Inconel 617[(SN = 1, $\sigma_b = 770$, $\delta = 60$) (Ref 10); (SN = 2, $\sigma_b = 755$, $\delta = 56$) (Ref 20); (SN = 3-8, $\sigma_b = 787$, $\delta = 67$) (Ref 21)]; Haynes 230 (SN = 9-12, $\sigma_b = 869$, $\delta = 63$) (Ref 21); Hastelloy C-22 (SN = 13-22, $\sigma_b = 843$, KV= 13.7) (Ref 14); SU263 (SN = 23-26, $\sigma_b = 950$, $\delta = 25$) (Ref 15); Inconel 718 (SN = 27-42, $\sigma_b = 1210$, KV= 50) (Ref 16)
Reduced activation F/M steel	MANET-II (SN = 43-53, $\sigma_b = 725$, $\delta = 15.4$, KV= 5.5) (Ref 22); OPTIFER-IV (SN = 54-60, KV= 9) (Ref 22); CLAM steel (SN = 61-72, $\sigma_b = 640$ (SN = 61-67), $\sigma_b = 751.5$ (SN = 68-72), $\delta = 28$, $\psi = 72.5$, KV= 250) (Ref 23,24); F82H (SN = 73-76, $\sigma_b = 678$, $\delta = 15.4$, KV= 12) (Ref 25); F82H (SN = 77-78, $\sigma_b = 644$, $\delta = 25$, $\psi = 78$, KV= 108) (Ref 26); EUROFER (SN = 79-82, KV= 9.47) (Ref 27)
Stainless steel	316L ((SN = 83-88, $\sigma_b = 515$, $\delta = 60$, KV= 103) (Ref 28), (SN = 89-90, $\sigma_b = 550$, $\psi = 28$) (Ref 29), (SN = 91-101, $\sigma_b = 640$, $\delta = 73.8$, KV= 280); 304 (SN = 102, $\sigma_b = 584$, $\delta = 32.6$, KV= 76.3) (Ref 30); 22Cr duplex (SN = 103, $\sigma_b = 767.7$, $\delta = 44$, KV= 294.3) (Ref 31); S136 (SN = 104-116, $\sigma_b = 1360$, $\delta = 7.8$)
Cast iron	FCD37 (SN = 117-127, KV= 20) (Ref 17)
ODS steel	MA 956 (SN = 128-133, $\sigma_b = 800$, $\psi = 27.1$) (Ref 32); PM2000 (SN = 134-137, KV= 0.12) (Ref 33)
Titanium alloy	IMI834 (SN = 138-145, $\sigma_b = 1029$, $\delta = 16$, KV= 5.4) (Ref 34); TC4 (SN = 146-160, KV= 22.5) (Ref 35); TC4 (SN = 161-165, $\sigma_b = 1039$, $\delta = 20.5$) (Ref 36); TC4 (SN = 166-178, $\sigma_b = 948$, $\delta = 14.7$, KV= 23.3); IMI 550 (SN = 179-181, $\sigma_b = 1000$, KV= 16.1, $\sigma_h = 570$) (Ref 37); IMI 318 (SN = 182, KV= 12.8, $\sigma_h = 415$) (Ref 37)
Intermetallic compound	Ti47Al2Cr002Si (SN = 183-190, $\sigma_b = 602$, $\delta = 1.5$) (Ref 38); γ -TiAl (SN = 191, $\tau_b = 476$) (Ref 39); Ti45Al5Nb (SN = 192, $\sigma_b = 1089.5$, $\delta = 3.88$) (Ref 18); Ti25Al10Nb (SN = 193-202, $\tau_b = 460$) (Ref 40)
Al alloy	Al2017 (SN = 203-213, $\sigma_b = 340$, $\delta = 12.5$, KV= 34.2) (Ref 41); Al7075 (SN = 215-220, $\sigma_b = 324$) (Ref 42); Al-Fe alloy (SN = 221-224, $\tau_b = 106.3$) (Ref 43)
Mg alloy	AZ31 ((SN = 225-231, $\tau_b = 88.7$) (Ref 44)
Where σ_b , τ_b , δ , ψ , KV are the tensile strength (MPa), shear strength (MPa), elongation (%), area reduction (%), and impact energy (J)	

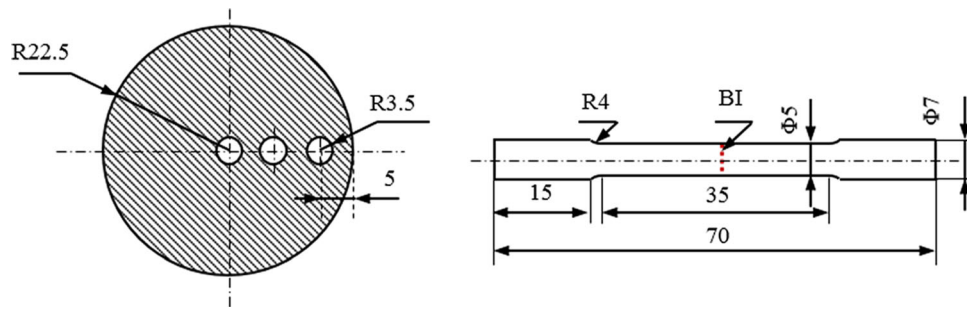


Fig. 1 Sampling locations and geometries of the specimens used by tensile test, where BI (the red dashed line) stands for the bonding interface

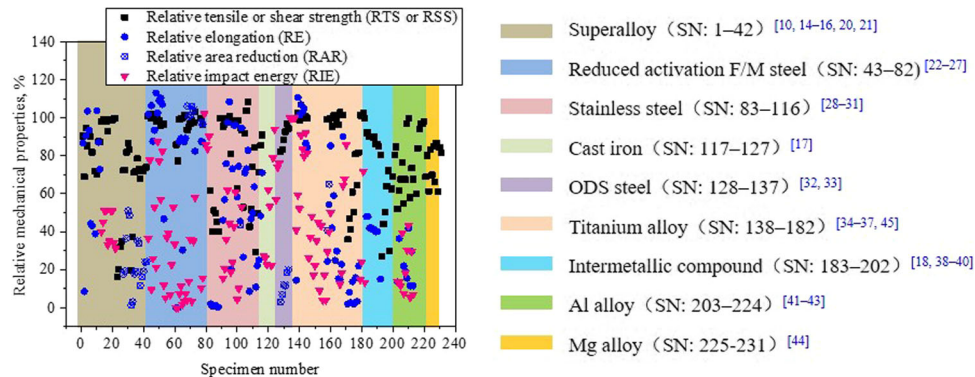


Fig. 2 Distribution of relative mechanical properties of diffusion bonded joints (ratio between the property of joint and that of the corresponding base alloy), where SN is the abbreviation of specimen number, and the same as that shown in Table 1

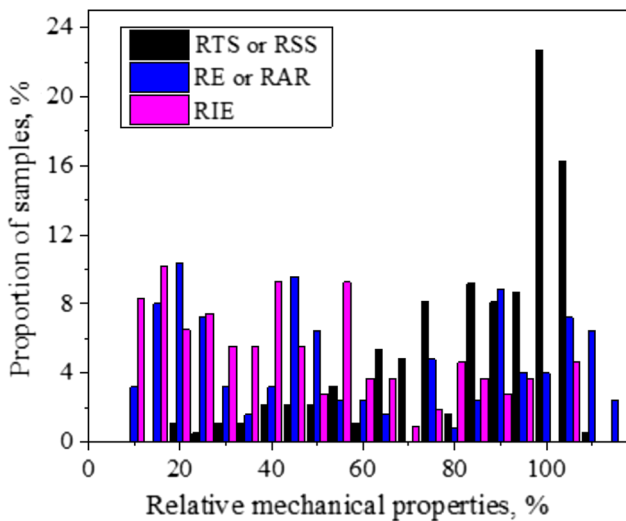


Fig. 3 Correlation between relative property values and its corresponding specimen ratios in the 231 joints investigated is shown in Table 1 and Fig. 2

compound and Al alloy are kept at a low level. Joint toughness, RIE, is the most highly dispersed property recognized in Fig. 2. Moreover, majority of RIE values are found to be less than 60%. Several joints, mostly ODS steel joints, have the RIE values near 100%.

As the data of high-temperature and fatigue properties are limited, the following analysis mainly focuses on the room-temperature strength, plasticity, and toughness of joints. Figure 3 shows the correlation between relative strength (RTS

or RSS), plasticity (RE or RAR), and toughness (RIE) values along with their corresponding specimen ratios in the 231 joints investigated.

The quantitative characterization shown in Fig. 3 further explicates the common features of diffusion bonded joints shown in Fig. 2(a), i.e., easy strengthening but difficult toughening. The proportion of specimens is 48.1, 21.7, and 7.83 for 0.9 of RTS (or RSS), RE (or RAR), and RIE, respectively.

4. Microstructure Features of Diffusion Bonded Joints

The difference in properties between the diffusion bonded joints and the corresponding base alloy resulted due to the differences in their microstructure. Thus, it can be regarded as the broad-sense defects of the joint, which are categorized into three types according to their morphologies. These are interfacial microvoids, bond line, and crystallographic mismatch. The effects of these three types of defects on the properties are discussed below.

4.1 Interfacial Microvoids

The interfacial microvoids were produced by asperities of the surface to be bonded. Its shrinkage was also the main object characterized in various diffusion bonding models since the 1970s (Ref 14,45-51). Consequently, they were regarded as the principle defect in diffusion bonding, especially for the materials that had not precipitated particles or had a certain

solid solubility at the bonding temperature, such as titanium alloys.

The degree of interfacial microvoids shrinkage is usually expressed by the bonded ratio in engineering. Figure 4(a), (b), (c), and (d) shows the typical morphology of microvoids in TC4 joints from our experiments (Ref 52). Before diffusion bonding, one of the sample surfaces to be bonded was polished to a roughness of Ra 0.03, and the other was lathed to Ra 0.4, Ra 0.8, Ra 1.6, and Ra 3.2. The microvoids shrinkage or the bonded ratio was generally enhanced by the increase in bonding temperature, pressure, or time.

Figure 4(e) shows the correlation between the bonded ratio and different mechanical properties of joints bonded at various

conditions (Ref 35, 52, 53). The experimental data in Fig. 4(e) emerged from different diffusion bonding conditions, the parameters of which are as follows: bonding temperature: 775-920 °C, bonding pressure: 0.5-10 MPa, bonding time: 5-120 min, and surface roughness: Ra 0.1-Ra 3.2. It is revealed that the values of RTS, RE, and RIE increase with bonded ratio. Nevertheless, RIE is the most sensitive indicator for evaluating the quality of joint, because the decrease in value of RIE is relatively more rapid when compared to those of RTS or RE, as the bonded ratio reduces from 100%. In comparison, RTS is highly insensitive to the microvoids as its value can easily reach to the level of base alloy. When the bonded ratio is 80%, the RTS is found to be at 100%.

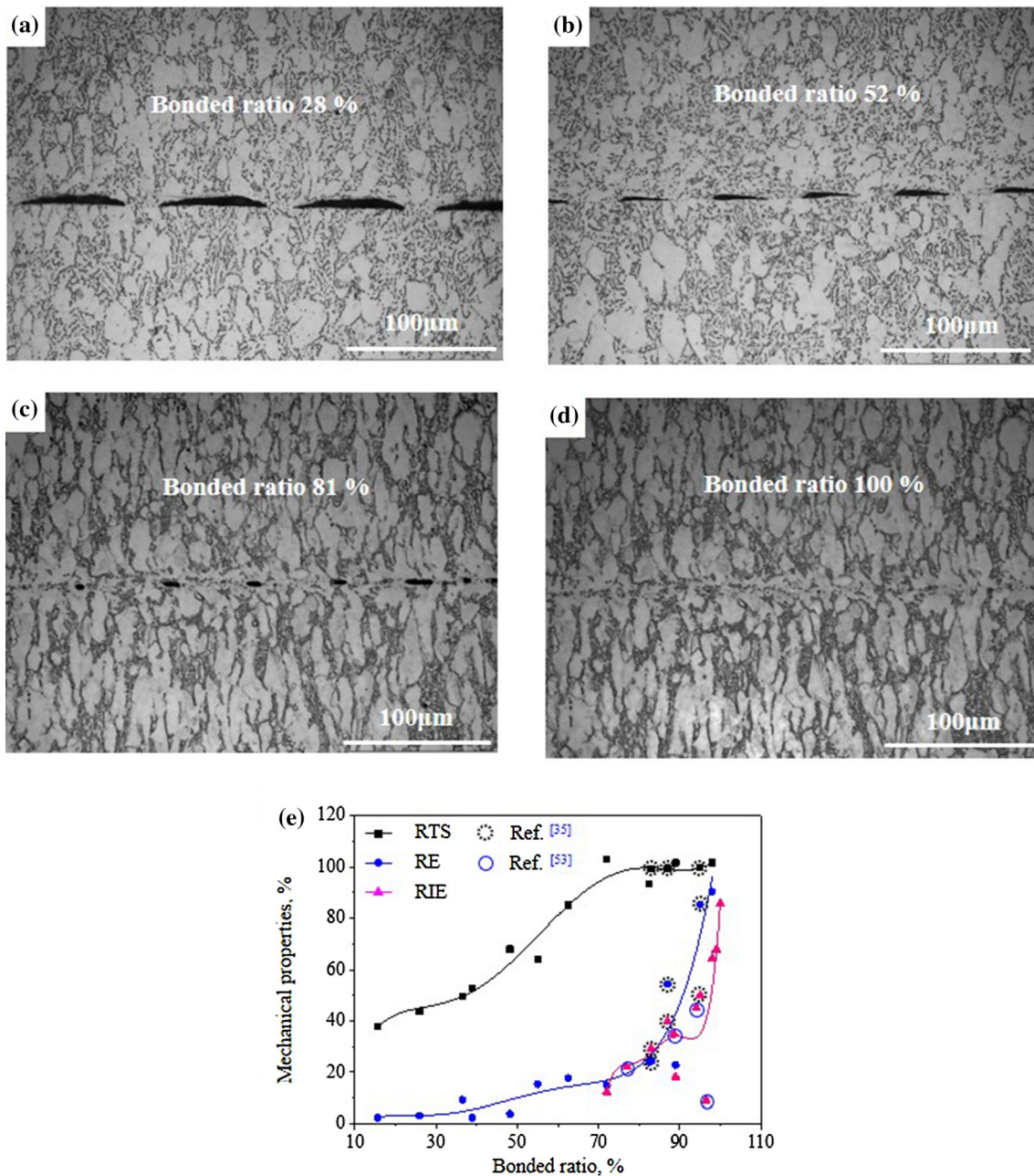


Fig. 4 Interfacial microvoids of titanium alloy TC4 joints diffusion bonded at 800 °C under 10 MPa for 15 min with the surface roughness of (a) Ra 3.2, (b) Ra 1.6, (c) Ra 0.8, and (d) Ra 0.4; and (e) the correlation between the bonded ratio of TC4 joint and its relative properties (Ref 52)

4.2 Bond Line

Bond line is a discernible line located at the original bonding interface. Although its existence has been reported in some studies (Ref 10,20-22,34), its effects on joint properties have rarely been reported.

Bond line is generally found in two types of alloys: the first where the alloys form precipitates on grain boundaries at high temperatures, such as 316L stainless steel, low activation martensitic (LAM) steel used in nuclear energy system and nickel-based superalloys. When these alloys are diffusion bonded, the precipitates are easily formed at the bonding interface because they have more vacancies than grain boundaries. These interfacial precipitations could pin grain boundaries and retard the grain growth across the initial bonding interface, subsequently, a bond line constituted by the interfacial precipitation particles and pinned grain boundaries appeared at the original bonding interface. The second type is one where the alloys could rapidly react with oxygen at room temperature and form a compact surface oxide film which is stable even at high temperatures, such as aluminum alloys. The oxide film was barely removed by the pre-bonding cleaning or heating in vacuum, thus transforming it into a bond line.

Figure 5 shows the bond line present in the joint of 316L stainless steel (see Fig. 5a and b) and the correlation between the bonded ratio and mechanical properties of the joint (see Fig. 5c). The joint shown in Fig. 5(a) and (b) was bonded at 1000 °C under 10 MPa for 60 min. Figure 5(c) brings together bonded ratio and mechanical properties of joints under different conditions, the parameters of which are as follows: bonding

temperature: 950-1100 °C, bonding pressure: 5-20 MPa, bonding time: 30-120 min, and surface roughness: Ra 0.1-Ra 3.2. Figure 5(a) indicates that bond line and microvoids can simultaneously appear at the bonding interface. However, the removal of bond line is more difficult than that of microvoids; thus, even when the bonded ratio reaches 100%, the bond line still exists, as shown in Fig. 5(b). The formation of the bond line in 316L stainless steel joint may have resulted from the precipitates of the chromium carbides ($M_{23}C_6$), laves phase (η), and σ -phase (Fe-Cr). In a similar study, where 316L stainless steel was aged at a high temperature, Sahlaoui and Sidhom (Ref 54) pointed out that these precipitates tend to form at grain boundaries. The comparison between Fig. 4(e) and 5(c) indicates that the 316L stainless steel joints present a similar tendency to the TC4 joints, i.e., RTS, RE, and RIE increase with the increase in bonded ratio. However, due to the existence of bond line, the increase in RIE with bonded ratio is comparatively slower in Fig. 5(c), where RIE is significantly lower than 100% even when the bonded ratio reaches 100%.

LAM steel is a group (7-9) Cr-(1-2) W-0.2 V-0.07 Ta-0.1 C steels which is generally used in nuclear energy systems due to its good irradiation and corrosion resistant performance as well as excellent mechanical properties at elevated temperatures. When LAM steel is heated to high temperatures, carbides of $M_{23}C_6$ and MC would precipitate at the grain boundaries (Ref 56,57). The precipitation of grain boundary carbide, though being a critical aspect in high-temperature properties of steels, could induce bond line during diffusion bonding (Ref 22-24). This characteristic of LAM steel is similar to that of the nickel-

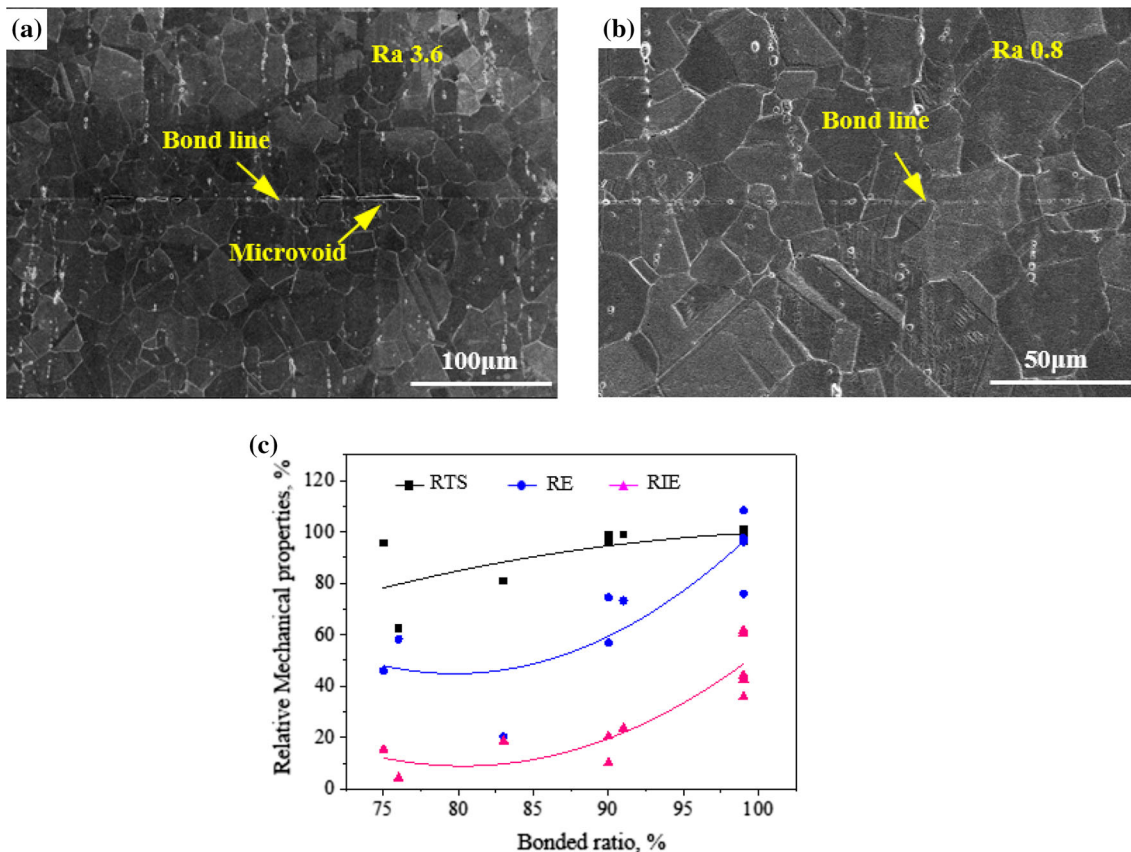


Fig. 5 Morphology of the bond line in the 316L stainless steel joint bonded at 1000 °C under 10 MPa for 60 min with the surface roughness of (a) Ra 3.6 or (b) Ra 0.8 and (c) the correlation between the bonded ratio of the 316L stainless steel joint and its relative properties (Ref 55)

based superalloys; thus, the bond line constituted by carbide precipitates and grain boundaries could also be found in superalloy joints (Ref 10,14,16,21).

Figure 6 further illuminates the effects of bond line on mechanical properties by demonstrating the relationships between strength (RTS) and plasticity or toughness (RE or RIE) for LAM steel joints (see Fig. 6a) and the nickel-based superalloy joints (see Fig. 6b). Figure 6 reveals two features. Firstly, the distributions of RE and RIE are scattered when RTS is around 100%. Secondly, RE is usually higher than RIE at the same RTS; moreover, most of the RIE values are less than 50%.

4.3 Crystallographic Mismatch

The defect of crystallographic mismatch, although rarely perceived and mentioned in the field of diffusion bonding research, generally impaired the joint properties. Crystallographic mismatch firstly refers to the significant grain size differences between the region near the bonding interface (i.e., interface region) and the region far from the bonding interface (i.e., base region). For the joint diffusion bonded at low temperature under high pressure, recrystallization occurs in the contact area of the joint without grain coarsening, where the grain size is less than that of base metal. The Hall–Petch relationship (Ref 58,59) shows that the yield stress is related to the grain size. The differences in grain size result in different yield stresses, which will cause the stress concentration and strain concentration at welded zone. Besides, the second meaning of crystallographic mismatch is the different lattice structure between the interface of joints and the base region, when the material is diffusion bonded by insertion of interlayer, especially in single crystal material such as single crystal superalloy. The polycrystalline interlayer has similar composition to single crystal base material. They show different responses behaviors during the same load, which will lead to stress concentration and strain concentration at welded zone. This type of mismatch will deteriorate the mechanical properties of the joint, especially in plasticity and toughness.

The crystallographic mismatch induced by grain size difference has adverse effects on joint properties. Figure 7 shows the microstructure of a tough pitch copper (99.9 wt. %) joint, which was diffusion bonded under 100 MPa at 400 °C for 60 min. Since the bonding temperature was less than the temperature [about 500 °C (Ref 60)] at which the grain growth

would be significant, the fine recrystallized grains (see Fig. 7a and b) and twin boundaries (see Fig. 7c and e) were produced around the bonding interface (marked in Fig. 7 as BI), and the diameter of recrystallized grains was only 1-7.5 μm (see Fig. 7d), which was 1-2 order of magnitude less than the grain diameter of the base metal (50-500 μm). Because the stacking fault energy of copper was relatively low, twin boundaries tended to occur in recrystallization grains during recrystallization annealing (Ref 61). Compared with traditional high-angle grain boundaries, twin boundaries had lower energy and generally showed high thermal and mechanical stability (Ref 62). The existence of twins could reduce dislocation mean free path, which led to the decrease in strength and the increase in plasticity. Furthermore, Fig. 7(a) shows the structure gradient between the interface area with fine crystal formed by recrystallization and the base metal with the relatively coarse crystal. Compared with the uniform deformation of the block material, stress concentration was formed at the interface during the tensile loading. Therefore, the elongation of the joint was only 23% that of the base metal, although the tensile strength of the joint (256.2 MPa) reached 98% that of the base metal.

5. Improvement of the Joint Mechanical Properties

Joint properties can be improved by the elimination or reduction of defects such as interfacial microvoids, bond line, and crystallographic mismatch.

However, only the elimination of interfacial microvoids has been intensively studied (Ref 14,45-51), which demonstrated that microvoid closure was enhanced by optimization of the processing parameters and decrease in the surface roughness.

The elimination of bond line can be conducted by the following two methods.

The first is the post-bond heat treatment. Sah et al. (Ref 21) found that the bond line in the Alloy 617 or Haynes 230 joint could partially be removed by post-bond heat treatments. This resulted in the increase in tensile strength and elongation of joints to a certain extent. Nevertheless, in most situations, the interfacial precipitates, the main factor for the formation of bond line, could not be removed completely by post-bond heat treatment. Subsequently, the recrystallized grain across the

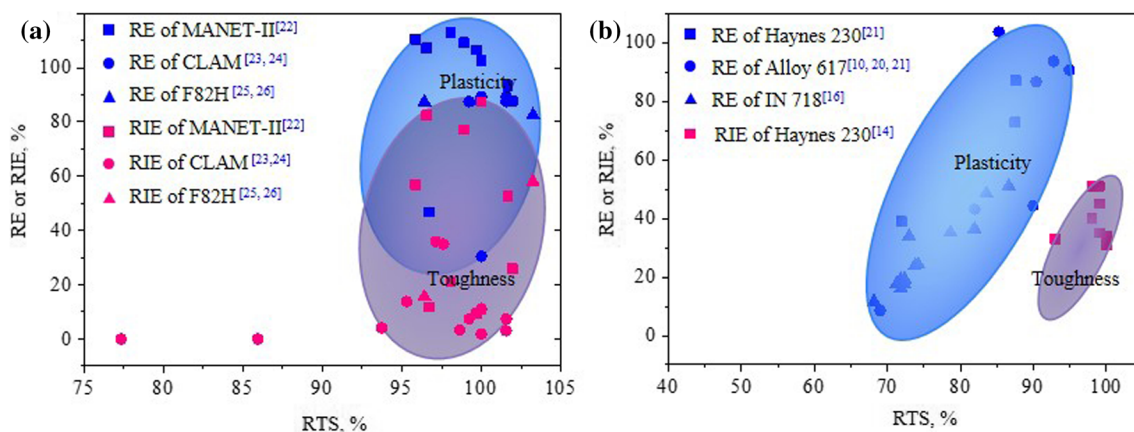


Fig. 6 Scattered distributions of the RE (or RIE) in the high RTS range presented by (a) the LAM steel joint and (b) nickel-based superalloy joint, which is mainly resulted from the existence of bond line

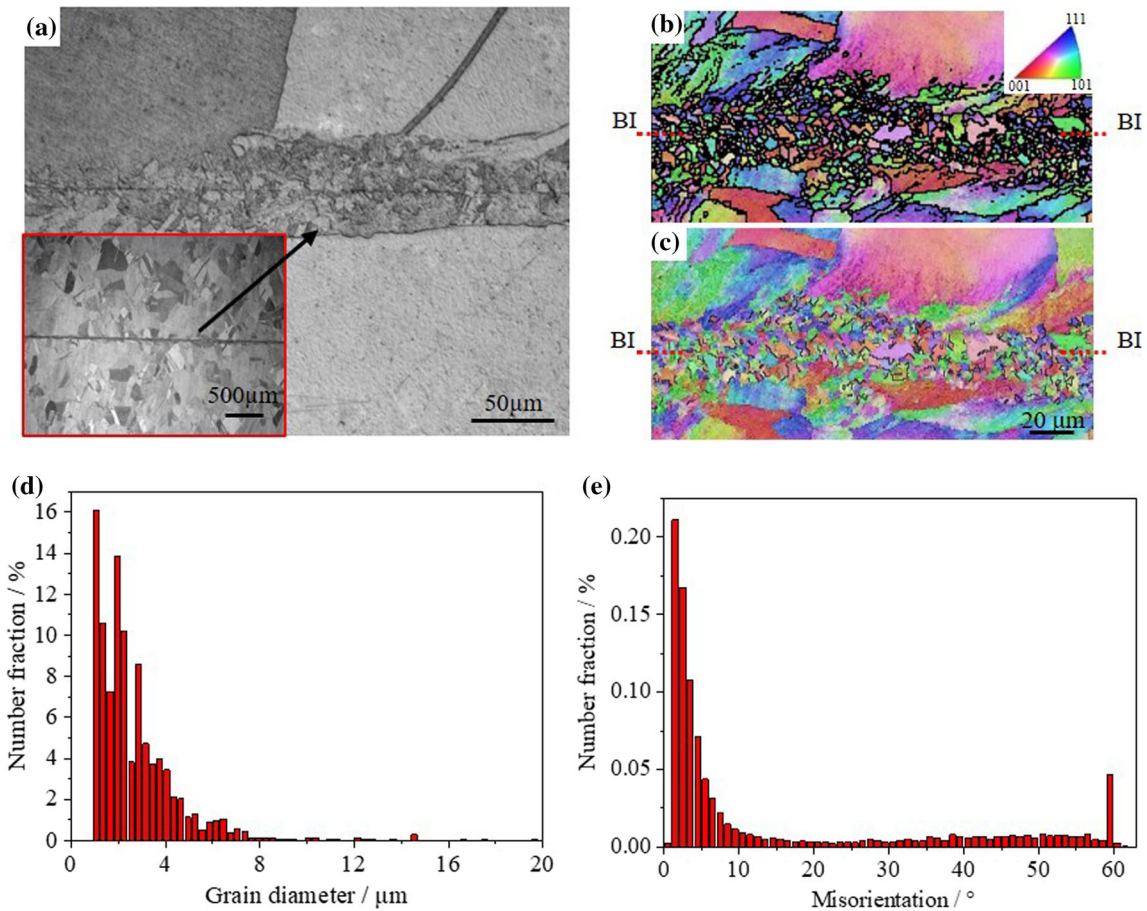


Fig. 7 Crystallographic mismatch presented by the copper joint, (a) the interfacial microstructure of joints, (b) the recrystallized grains around the bonding interface (i.e., BI) and (c) twin boundaries in the cross-sectional electron backscatter diffraction (EBSD) inverse-pole figure (IPF) map, (d) the distribution of the recrystallized grains around the bonding interface, and (e) the misorientation angle distribution of the joint

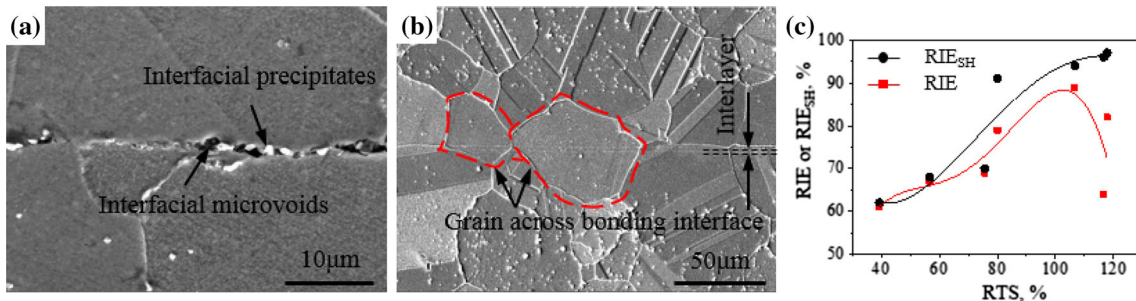


Fig. 8 SEM images of (a) the bond line in directly bonded GH4099 joint and (b) the recrystallized grains across the bonding interface in the GH4099 joint bonded with 2-µm thick Ni interlayer, and (c) the relationship between the RTS and RIE (or RIE_{SH}) presented by GH4099 joints bonded with Ni interlayer (Ref 64)

bonding interface was still retarded by the residual precipitates; thus, the elimination of bond line produced by post-bond heat treatment was rather limited. Comparatively, it exhibited more effects than to insert an interlayer which could suppress the formation of interfacial precipitates.

The second is insertion of the interlayer, which can suppress the formation of interfacial precipitates. Figure 8 shows the joints of GH4099 alloy that is a precipitation-hardened nickel-based superalloy developed by China, whose composition is similar to Russia's ЭП693. In the joint directly diffusion bonded

under 10 MPa at 1120 °C for 60 min (see Fig. 8a), the bond line constituted by interfacial microvoids and precipitates ($M_{23}C_6$) can be easily detected, and thus, the mechanical properties of this directly bonded joint were extremely poor, to an extent that it broke during the machining process. In contrast, the joint bonded with a 2-µm thick pure Ni interlayer (see Fig. 8b) had a bond line that almost disappeared, because the formation of interfacial precipitates of $M_{23}C_6$ was suppressed by the certain solid solubility of carbon in nickel at high temperatures (about 0.25 wt. % at 1120-1160 °C) (Ref

Table 2 The influencing degree of microstructure features on mechanical properties of diffusion bonding joints

	Tensile strength	Elongation (or area reduction)	Impact toughness
Interfacial microvoids	○	○○	○○○
Bond line	○	○○	○○○○
Crystallographic mismatch	×	○○	○○○

Where the degree of influence on the mechanical properties is expressed by different symbols; × means no influence, ○ means the minimum degree of influence and ○○○○ means the maximum degree of influence

63). After that, there were no precipitates that could retard the growth of recrystallized grain across the bonding interface, as indicated in Fig. 8(b). However, the bond line in GH4099 joint was removed by the insertion of pure Ni interlayer. Figure 8(c) shows the relationship between RIE and RTS, which is quite different from the scattered distribution of RTS due to the existence of bond line, as shown in Fig. 6. The joints shown in Fig. 8(c) were bonded at 1200-1600 °C under 4-10 MPa for 60-120 min with a 2-20- μ m thick Ni interlayer (Ref 64). Moreover, the beneficial effects of bond line elimination can be more clearly demonstrated by the monotonical increase in RIE_{SH} with RTS shown in Fig. 8(c), where RIE_{SH} is the ratio between impact energy of the joint and that of the base alloy undergoing the same heating process. The highest value reached by RIE_{SH} is 96%. This phenomenon suggests that the microstructure of a joint can be very similar to that of the base alloy undergoing the same heating process, and the RIE value decreases as RTS increases from 100 to 120%, which results from the microstructure degradation produced by the heating process of grain coarsening.

Elimination of the bond line can also be done by changing the surface treatment or preventing the dissolution of interfacial oxides at the joint that could rapidly react with oxygen at room temperature and form a compact surface oxide film which is stable even at high temperatures, such as aluminum alloy. Measures for reducing the influence of surface oxide include increasing the plastic deformation at the interface (Ref 65,66), adding active metal (Mg, Zn, Li, Ge, etc.) as an interlayer which can react with oxide film (Ref 67-69), using argon ion beam to remove the oxide film for creating a clean surface (Ref 70), and coating organic solution on the welding surface to shield the bonding surface right after the cleaning (Ref 71-73). For diffusion bonding, ethanol (Ref 71), acetone, styrene (C₆H₅-CH=CH₂), polyvinyl benzene (Ref 72), and ethylene glycol monomethyl ether (HO-CH₂-CH₂-O-CH₃) (Ref 73) have been reported to protect the aluminum surface from secondary oxidation. Furthermore, in our previous study, a self-assembled monolayer (1-hexyl mercaptan) was used on aluminum surfaces to prevent the secondary oxidation after pre-bonding treatment (Ref 74). Three different pre-bonding surface treatments were employed in the diffusion bonding joint of AA6063/AA6063, which were as-cleaned, ethanol adsorbed and self-assembled monolayer passivated. These three types of joints with bond ratios of 64.1, 84.7, and 97.4% showed the corresponding joint strengths of 129.2, 147.8, and 165.2 MPa, respectively. Furthermore, the surface passivated by self-assembled monolayer had very few voids at the bonding interface. The joint had a bond ratio of 97.4% along with an elongation of 20.4% which is very close to that of the base metal and is considered as an equal-strength bonding.

The method for eliminating crystallographic mismatch has rarely been reported since very little attention is paid to it in the traditional study of diffusion bonding; thus, future studies should focus on removal of the crystallographic mismatch to further increase and strengthen the properties of the joint, especially those used under dynamic and/or high-temperature loading.

For better evaluation, the influencing degree of these three types of interfacial characteristics on mechanical properties of diffusion bonding joints is summarized in Table 2, which shows that tensile strength of diffusion bonding joints is not sensitive to interfacial microvoids and bond line, while the crystallographic mismatch almost has no effect on tensile strength. Nevertheless, the elongation (or area reduction) is more sensitive to these types of microstructure features as compared to tensile strength. At the same time, it can be observed that impact toughness is the most sensitive indicator for evaluation of joints' quality since it is highly perceptive toward interfacial microvoids, bond line, and crystallographic mismatch. Figures 2, 4(e), 5(c) and 6 explain that when the bonded ratio is 80%, RTS is already 100%. When the bonded ratio increases to 100%, RIE reaches 90% as shown in Fig. 4. However, due to the existence of bond line, even though RTS reaches 100%, RIE is significantly lower than 100% (i.e., 30-50%) as shown in Fig. 5. Therefore, the impact toughness is more sensitive to bond line as compared to interfacial microvoids and crystallographic mismatch. Furthermore, with heat treatment or by application of an interlayer, the RIE_{SH} (ratio between impact energy of the joint and that of the base alloy undergoing the same heating process) value increases from 90 to 96% as the RTS increases from 100 to 120% (see Fig. 8). This indicates that the elimination of bond line can significantly improve the joint toughness.

6. Conclusions

The common features of the mechanical properties of diffusion bonded joints and their corresponding microstructure features were analyzed by the normalization of the properties of 29 types of alloys which were joined by diffusion bonding (231 specimens). The following conclusions were drawn:

- (1) The tensile (or shear) strength of the joint was easily able to attain the same value as that exhibited by the base alloy, where the ductility (i.e., elongation or area reduction) and toughness of the joint were significantly lower than those of the base alloy on several occasions.
- (2) The microstructural difference between the joints and the base alloys was found to be the main reason for the

relatively lower properties of the joint; based on this difference, the joint defects were classified into three types, i.e., interfacial microvoids, bond line, and crystallographic mismatch.

- (3) The interfacial microvoids had a greater effect on the joint ductility or toughness than on the joint strength. Moreover, when the microvoids were completely eliminated (i.e., 100% bonded ratio), the joint elongation and impact energy attained approximately equal values as those of the base alloy.
- (4) The existence of the bond line significantly decreased the joint ductility and toughness; however, it did not affect the joint strength and led to a scattering of the distributions of the joint elongation and impact energy. Furthermore, the impact energy of the joint barely reached the level of the base alloy, even when the bonded ratio or RTS was approximately 100%.

Acknowledgments

This work was supported by the National Natural Science Foundations of China (Grant Nos. U1737205 and 51975480) and the State Key Laboratory of Solidification Processing (NWPUP, China) (Grant No. 2019-TS-09).

References

1. Y. Xun and M. Tan, Applications of superplastic forming and diffusion bonding to hollow engine blades, *J. Mater. Process. Technol.*, 2000, **99**, p 80–85
2. D. Serra. Superplastic forming applications on aero engines. A review of ITP manufacturing processes, in *6th EUROSPF conference. EuroSPF08, Carcassonne, France*, 2008
3. X. Zhou, Y. Liu, L. Yu, C. Liu, G. Sui, and J. Yang, Uniaxial diffusion bonding of CLAM/CLAM steels: Microstructure and mechanical performance, *J. Nucl. Mater.*, 2015, **461**, p 301–307
4. J. Chen, C. Liu, C. Wei, Y. Liu, and H. Li, Study on microstructure and mechanical properties of direct diffusion bonded low-carbon RAFM steels, *J. Mater. Process.*, 2019, **43**, p 192–199
5. B.A. Robbers, B.J. Anderson, W.A. Hayes, R.A. Hewitt, and M.G. Brown. Platelet devices—limited only by one’s imagination, in *42nd AIAA/ASME/SAE/ASEE Joint Propulsion Conference & Exhibit Sacramento, California*. 2006
6. T. Nguentat, W. Hayes, T. Meland, and E. Veith. Fabrication of a liquid rocket combustion chamber liner of advanced copper alloy groop-84 via formed platelet liner technology, in *42nd AIAA/ASME/SAE/ASEE Joint Propulsion Conference & Exhibi*, 2006
7. J.P. Fleuriel, J. Chase, P. Gogna, S. Firdosy, B.C. Li, N. Keyawa, G.H. Nakatsukasa, and B. Nesmith. 1 kW small fission heat pipe-cooled thermoelectric power system design concept and technology maturation, in *11th International Energy Conversion Engineering Conference*, San Jose, CA USA, 2013
8. A.P. London, A.H. Epstein, and J.L. Kerrebrock, High-pressure bipropellant microrocket engine, *J. Propul. Power*, 2001, **17**, p 780–787
9. X. Zhang, S. Shi, R.N. Christensen, and X. Sun, Review on mechanical design of printed circuit heat exchangers, in *Proceedings of 25th ICONE*, Shanghai, China, 2017
10. X. Li, D. Kininmont, R.L. Pierres, and S.J. Dewson. Alloy 617 for the high temperature diffusion-bonded compact heat exchangers, in *Proceedings of ICAPP*, Anaheim, CA USA, 2008
11. D. Southall and S.J. Dewson, Innovative compact heat exchangers, in *Proceedings of ICAPP10*, San Diego, CA, USA, 2010
12. J.K. Min, J.H. Jeong, M.Y. Ha, and K.S. Kim, High temperature heat exchanger studies for applications to gas turbines, *Heat Mass Transf.*, 2009, **46**, p 175–186
13. H. Zhang, J.L. Li, P.Y. Ma, J.T. Xiong, and F.S. Zhang, Study on microstructure and impact toughness of TC4 titanium alloy diffusion bonding joint, *Vacuum*, 2018, **152**, p 272–277
14. W.W. Basuki, O. Kraft, and J. Aktaa, Optimization of solid-state diffusion bonding of Hastelloy C-22 for micro heat exchanger applications by coupling of experiments and simulations, *Mater. Sci. Eng. A Struct.*, 2012, **538**, p 340–348
15. B. Ravisankar, J. Krishnamoorthi, S.S. Ramakrishnan, and P.C. Angelo, Diffusion bonding of SU 263, *J. Mater. Process. Technol.*, 2009, **209**, p 2135–2144
16. G. Zhang, R.S. Chandel, and H.P. Seow, Solid state diffusion bonding of Inconel 718, *Sci. Technol. Weld. Join.*, 2001, **6**, p 235–239
17. S. Mukae, K. Nishio, M. Katoh, and N. Nakamura, Impact characteristics of diffusion bonds of ferritic spheroidal graphite cast iron, *Trans. Jpn. Weld. Soc.*, 1990, **21**, p 41–51
18. D. Herrmann and F. Appel, Diffusion bonding of γ (TiAl) alloys: influence of composition, microstructure, and mechanical properties, *Metall. Mater. Trans. A*, 2009, **40**, p 1881–1902
19. Z. Wu, J. Mei, W. Voice, S. Beech, and X. Wu, Microstructure and properties of diffusion bonded Ti-6Al-4V parts using brazing-assisted hot isostatic pressing, *Mater. Sci. Eng. A Struct.*, 2011, **528**, p 7388–7394
20. S.K. Mylavarapu, X. Sun, R.N. Christensen, R.R. Unocic, R.E. Glosup, and M.W. Patterson, Fabrication and design aspects of high-temperature compact diffusion bonded heat exchangers, *Nucl. Eng. Des.*, 2012, **249**, p 49–56
21. I. Sah, D. Kim, H.J. Lee, and C. Jang, The recovery of tensile ductility in diffusion-bonded Ni-base alloys by post-bond heat treatments, *Mater. Des.*, 2013, **47**, p 581–589
22. K. Schleisiek, T. Lechler, L. Schäfer, and P. Weimar, Diffusion welding parameters and mechanical properties of martensitic chromium steels, *J. Nucl. Mater.*, 2000, **283–287**, p 1196–1200
23. C. Li, Q. Huang, P. Zhang, and F.D.S. Team, Preliminary experimental study on Hot Isostatic Pressing diffusion bonding for CLAM/CLAM, *Fusion Eng. Des.*, 2007, **82**, p 2627–2633
24. C. Li, Q. Huang, and P. Zhang, Effect of surface preparation on CLAM/CLAM hot isostatic pressing diffusion bonding joints, *J. Nucl. Mater.*, 2009, **386–388**, p 550–552
25. K. Furuya, E. Wakai, M. Ando, T. Sawai, A. Iwabuchi, K. Nakamura, and H. Takeuchia, Tensile and impact properties of F82H steel applied to HIP-bond fusion blanket structures, *Fusion Eng. Des.*, 2003, **69**, p 385–389
26. T. Hirose, K. Shiba, M. Ando, M. Enoda, and M. Akiba, Joining technologies of reduced activation ferritic/martensitic steel for blanket fabrication, *Fusion Eng. Des.*, 2006, **81**, p 645–651
27. A.V.D. Weth, H. Kempe, J. Aktaa, and B. Dafferner, Optimization of the EUROFER uniaxial diffusion weld, *J. Nucl. Mater.*, 2007, **367–370**, p 1203–1207
28. Z.L. An, W.L. Luan, F.Z. Xuan, and S.T. Tu, High temperature performance of 316L-SS joint produced by diffusion bonding, *Key Eng. Mater.*, 2005, **297–300**, p 2795–2799
29. S. Li, F. Xuan, and S. Tu, Fatigue damage of stainless steel diffusion-bonded joints, *Mater. Sci. Eng. A Struct.*, 2008, **480**, p 125–129
30. M.J. Cox, R.W. Carpenter, and M.J. Kim, Interface nanochemistry effects on stainless steel diffusion bonding, *Metall. Mater. Trans. A*, 2002, **33**, p 437–442
31. X. Li, Development and qualification of diffusion bonding procedures for microchannel heat exchangers, in *ASME 31st International Conference on Ocean, Offshore and Arctic Engineering*, 2012
32. Z. Guoge and R.S. Chandel, Solid state diffusion bonding of Incoloy MA 956 to itself, *J. Mater. Sci.*, 2003, **22**, p 1693–1695
33. W. Sittel, W.W. Basuki, and J. Aktaa, Diffusion bonding of the oxide dispersion strengthened steel PM2000, *J. Nucl. Mater.*, 2013, **443**, p 78–83
34. A. Wisbey and P.G. Partridge, Diffusion bonding of high temperature titanium alloy IMI, 834, *Mater. Sci. Technol. Lond.*, 1993, **9**, p 441–444
35. J.M. Gómez de Salazar, A. Ureña, and J.G. Carrión, Charpy impact test of Ti-6Al-4V joints diffusion welded at low temperature, *Scr. Mater.*, 1996, **35**, p 479–484
36. S.J. Tuppen, M.R. Bache, and W.E. Voice, Structural integrity of diffusion bonds in Ti-6Al-4V processed via low cost route, *Mater. Sci. Technol. Lond.*, 2006, **22**, p 1423–1430

37. T.S. Baker and P.G. Partridge, Fatigue and impact strength of diffusion bonded titanium alloy joints, in *Proceedings of an international conference on diffusion bonding(7-8th)*, Cranfield, 1987
38. W. Glatz and H. Clemens, Diffusion bonding of intermetallic Ti-47Al-2Cr-0.2-Si sheet material and mechanical properties of joints at room temperature and elevated temperatures, *Intermetallics*, 1997, **5**, p 415–423
39. G. Cam and M. Kocak, Diffusion bonding of investment cast γ -TiAl, *J. Mater. Sci.*, 1999, **34**, p 3345–3354
40. Y. Wu, W. Wei, and C.H. Koo, Diffusion bonding of Ti-25Al-10Nb alloy, *Sci. Technol. Weld. Join.*, 1998, **3**, p 97–104
41. M. Cailler, O. Debouz, M. Dannawi, and T. Latouche, Mechanical characterization by dynamical tensile loading of 2017 aluminium alloy joints welded by diffusion bonding, *J. Mater. Sci.*, 1991, **26**, p 4997–5003
42. Y. Huang, F.J. Humphreys, N. Ridley, and Z.C. Wang, Diffusion bonding of hot rolled 7075 aluminium alloy, *Mater. Sci. Technol. Lond.*, 1998, **14**, p 405–410
43. H. Somekawa, T. Tanaka, H. Sasaki, K. Kita, A. Inoue, and K. Higashi, Diffusion bonding in ultra fine-grained Al-Fe alloy indicating high-strain-rate superplasticity, *Acta Mater.*, 2004, **52**, p 1051–1059
44. H. Somekawa, H. Hosokawa, H. Watanabe, and K. Higashi, Diffusion bonding in superplastic magnesium alloys, *Mater. Sci. Eng. A Struct.*, 2003, **339**, p 328–333
45. G. Garmong, N.E. Paton, and A.S. Argon, Attainment of full interfacial contact during diffusion bonding, *Metall. Trans. A*, 1975, **6**, p 1269–1279
46. B. Derby and E.R. Wallach, Theoretical model for diffusion bonding, *Met Sci*, 1982, **16**, p 49–56
47. A. Hill and E.R. Wallach, Modelling solid-state diffusion bonding, *Acta Metall.*, 1989, **37**, p 2425–2437
48. Y. Takahashi, K. Takahashi, and K. Nishiguchi, A numerical analysis of void shrinkage processes controlled by coupled surface and interface diffusion, *Acta Metall.*, 1991, **39**, p 3199–3216
49. H. Li, M.Q. Li, and P.J. Kang, Void shrinking process and mechanisms of the diffusion bonded Ti-6Al-4V alloy with different surface roughness, *Appl. Phys. A Mater.*, 2016, **122**, p 1–8
50. G.Q. Wu, Z.F. Li, G.X. Luo, H.Y. Li, and Z. Huang, Dynamic simulation of solid-state diffusion bonding, *Mater. Sci. Eng. A Struct.*, 2007, **452–453**, p 529–535
51. N. Orhan, M. Aksoy, and M. Eroglu, A new model for diffusion bonding and its application to duplex alloys, *Mater. Sci. Eng. A Struct.*, 1999, **271**, p 458–468
52. L. Yuan, J.T. Xiong, Y. Peng, Z.Z. Li, and J.L. Li, Modeling void closure in solid-state diffusion bonding of TC4 alloy, *Vacuum*, 2020, **173**, p 109120
53. M. Ohsumi, S. Kiyotou, and M. Sakamoto, The application of diffusion welding to aircraft titanium alloys, *Trans. ISIJ*, 1985, **25**, p 513–520
54. H. Sahlaoui and H. Sidhom, Experimental investigation and analytical prediction of σ -phase precipitation in AISI, 316L austenitic stainless steel, *Metall. Mater. Trans. A*, 2013, **44**, p 3077–3083
55. H. Zhang, J.L. Li, P.Y. Ma, J.T. Xiong, and F.S. Zhang, Effect of grain boundary migration on impact toughness of 316L diffusion bonding joints, *Mater. Res. Express*, 2019, **6**, p 076535
56. P. Liu, M. Zhao, Y. Zhu, J. Bai, F. Wan, and Q. Zhan, Effects of carbide precipitate on the mechanical properties and irradiation behavior of the low activation martensitic steel, *J. Alloy Comp.*, 2013, **579**, p 599–605
57. R. Ravikiran, S. Mythili, S. Raju, T. Saroja, and E.Rajendrakumar Jayakumar, Influence of W and Ta content on microstructural characteristics in heat treated 9Cr-reduced activation ferritic/martensitic steels, *Mater. Charact.*, 2013, **84**, p 196–204
58. D.V. Wilson and J.A. Chapman, Effects of preferred orientation on the grain size dependence of yield strength in metals, *Philos. Mag.*, 1963, **8**, p 1543–1551
59. R.W. Armstrong and Q. Li, Dislocation mechanics of high-rate deformations, *Metall. Mater. Trans. A*, 2015, **46**, p 4438–4453
60. J. Gupta, J.M.E. Harper, J. Mauer, P.G. Blauner, and D.A. Smith, Focused ion beam imaging of grain growth in copper thin films, *Appl. Phys. Lett.*, 1996, **61**, p 663–665
61. T. Baudin, A.L. Etter, and R. Penelle, Annealing twin formation and recrystallization study of cold-drawn copper wires from EBSD measurements, *Mater. Charact.*, 2007, **58**, p 947–952
62. K. Lu, L. Lu, and S. Suresh, Strengthening materials by engineering coherent internal boundaries at the nanoscale, *Science*, 2009, **324**, p 349–352
63. M. Singleton and P. Nash, The C-Ni (carbon-nickel) system, *J. Phase Equilib.*, 1989, **10**, p 121–126
64. J.T. Xiong, L. Yuan, Y. Zhu, H. Zhang, and J.L. Li, Diffusion bonding of nickel-based superalloy GH4099 with pure nickel interlayer, *J. Mater. Sci.*, 2019, **54**, p 6552–6564
65. H.Y. Wu, S. Lee, and J.Y. Wang, Solid-state bonding of iron-based alloys, steel-brass, and aluminum alloys, *J. Mater. Process. Technol.*, 1998, **75**, p 173–179
66. A.S. Zuruzi, H. Li, and G. Dong, Effects of surface roughness on the diffusion bonding of Al alloy 6061 in air, *Mater. Sci. Eng. A*, 1999, **270**, p 244–248
67. L.M. Zhao and Z.D. Zhang, Effect of Zn alloy interlayer on interface microstructure and strength of diffusion-bonded Mg-Al joints, *Scr. Mater.*, 2008, **58**, p 283–286
68. E.R. Maddrell, R.A. Ricks, and E.R. Wallach, Diffusion bonding of aluminum alloys containing lithium and magnesium, *Proc. Conf. Alum. Lithium*, 1989, **5**, p 451–460
69. A.A. Shirzadi and G. Saindrenan, New method for flux free diffusion brazing of aluminium alloys using liquid gallium, *Sci. Technol. Weld. Join.*, 2003, **8**, p 149–153
70. H. Chen, J. Cao, X. Tian, R. Li, and J. Feng, Low-temperature diffusion bonding of pure aluminum, *Appl. Phys. A Mater.*, 2013, **113**, p 101–104
71. Y.E. Wu and Y.L. Lo, Surface protection for AA8090 aluminum alloy by diffusion bonding, *Theor. Appl. Fract. Mech.*, 2002, **38**, p 71–79
72. Y. Huang, N. Ridley, F.J. Humphreys, and J.Z. Cui, Diffusion bonding of superplastic 7075 aluminum alloy, *Mater. Sci. Eng. A*, 1999, **266**, p 295–302
73. W.W. Li, M.Sc. thesis, Research on diffusion bonding technology of 5083 aluminum alloy. Nanjing University of Aeronautics and Astronautics, PRC (2007) (in Chinese)
74. H. Zhang, J.L. Li, C.S. Wang, J.T. Xiong, and F.S. Zhang, Equal-strength precision diffusion bonding of AA6063 aluminum alloy with the surface passivated by a self-assembled monolayer, *Int. J. Mater. Res.*, 2017, **108**, p 571–577

Publisher's Note Springer Nature remains neutral with regard to jurisdictional claims in published maps and institutional affiliations.